diffusion-fundamentals.org

Nb$_3$Sn Targets Synthesis via Liquid Tin Diffusion for Thin Films Depositions

Matteo Zanierato,[1,2] Oscar Azzolini,[1] Jonathan Cavazzani,[2]
Eduard Chyhyrynets,[1,2] Vanessa Garcia Diaz,[1] Antonella Glisenti,[2]
Giorgio Keppel,[1] Nico Ragazzo,[1,2] Fabrizio Stivanello,[1] Cristian Pira,[1]

[1] Legnaro National Laboratories (LNL) - Istituto Nazionale di Fisica Nucleare (INFN), Legnaro, Italy
[2] Università degli Studi di Padova (UNIPD) – Dipartimento di Scienze Chimiche (DISC), Padova, Italy

Corresponding author: Matteo Zanierato, Legnaro National Laboratories (LNL) - Istituto Nazionale di Fisica Nucleare (INFN), Legnaro, Italy, e-mail: matteo.zanierato@lnl.infn.it

Abstract

The deposition of superconducting Nb$_3$Sn on copper accelerating cavities is interesting for the higher thermal conductivity of copper compared to common Nb substrates. The better heat exchange would allow the use of cryocoolers reducing cryogenic costs and the risk of thermal quench [1]. The magnetron sputtering technology allows the deposition of Nb$_3$Sn on substrates different than Nb, however the coating of substrates with complex geometry (such as elliptical cavities) may require target with non-planar shape, which are difficult to realize with classic powder sintering techniques. In this work, the possibility of using the Liquid Tin Diffusion (LTD) technique to produce sputtering targets is explored. The LTD technique is a wire fabrication technology, already developed in the past at LNL for superconducting radio frequency (SRF) applications [2], that allows the deposition of very thick and uniform coating on Nb substrates even with complex geometries [3]. Improvements in LTD process, proof of concept of a single use LTD target production, and characterization of the Nb$_3$Sn film coated by DC magnetron sputtering with these innovative targets are reported in this work.

Keywords

Liquid tin diffusion, sputtering, Nb$_3$Sn, SRF, accelerating cavities.

1. Introduction

The thin film technology deposition of Nb_3Sn represents an interesting perspective for superconducting radio frequency (SRF) applications.

The Nb_3Sn shows theoretical performance, as critical temperature and accelerating gradient, higher respect to Nb. The Nb_3Sn thin films on Nb bulk cavities produced by Vapor Tin Diffusion (VTD) are the state of the art [4], but there is a strong interest in growing Nb_3Sn on a Cu substrate by PVD techniques because of its higher thermal conductivity [1]. The sputtering is the most promising PVD technique [5,6], but it requires the presence/use of a cylindrical Nb_3Sn cathode that must be cooled. Nb_3Sn is extremely brittle and is not machinable. On the other hand, powder sintering is not suitable for complex geometry targets.

One possible solution is the production of the targets by growing thick films of Nb_3Sn on a niobium substrate with Liquid Tin Diffusion (LTD) technique [3].

The LTD technology has been deeply studied at LNL from 2005 to 2009 [2]. The LTD allows the formation of thick films on niobium substrates by direct immersion in molten tin. The films deposited with DC magnetron sputtering are analysed and the characteristics are correlated with the synthesis process via LTD.

The LTD technique allows the coating on substrates with various geometry. The synthesis of cylindrical targets for 6 GHz (10 cm) and 1.3 GHz (50 cm) cavities at industrial level is relatively easy to scale, indeed, this diffusive technique is a variation of hot-dip galvanisation.

2. Method and Materials

The material under study is Nb_3Sn, a superconductor compound synthetized on bulk Nb substrate by immersion in molten tin (Sn 99.99%). The phase diagram is shown in Fig. 1 [7]. It is essential to operate at temperatures above 930°C for the formation of only the Nb_3Sn phase defined as A15. A rapid thermal quench minimises the formation of spurious phases due to excess Sn on the sample surface.
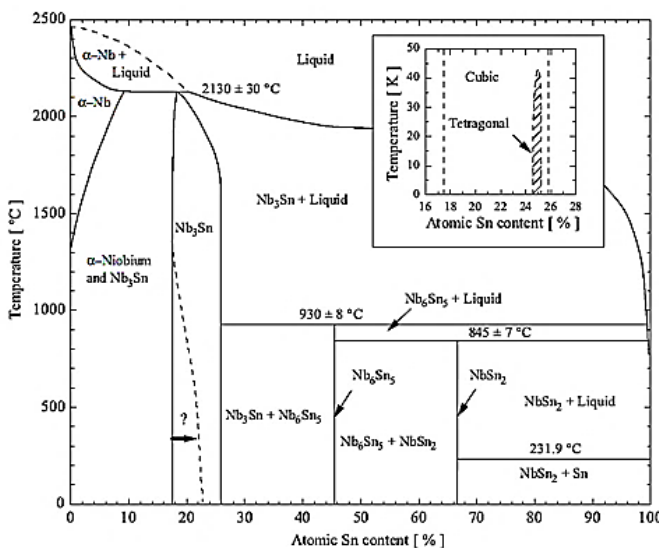

Fig. 1: Binary phase diagram of the Nb-Sn system from A. Godeke [7].

Two types of samples are studied: rectangular Nb bulk samples (30x15x3 mm) and one-inch diameter planar targets 3 mm thick. The niobium substrates are subjected to ultrasonic bath and subsequent Buffer Chemical Polishing (BCP) [8] HF: HNO_3: H_3PO_4 in a 1:1:2 ratio from five to ten minutes. The substrates prepared for nucleation are subsequently anodized at 20 V for one minute in NaOH solution to form a 70 nm Nb_2O_5 layer. For each run, 2 samples at a time have been used: one anodized and one just polished with BCP to evaluate possible change in the film growth.

The LTD system consists of an ultra-high vacuum pumping system, a linear manipulator, a furnace used for heating the crucible containing the tin, a furnace used for annealing of the samples, and a water jacket. The main chamber is made of Inconel and all internal parts are made of niobium. The samples are fixed to the manipulator by niobium wires. The system is heated and evacuated to a base pressure of 10^{-8} mbar [3]. The optimised process is divided into 6 steps as shown in Fig. 2. The general temperature scheme of the furnaces is shown in Fig. 3.
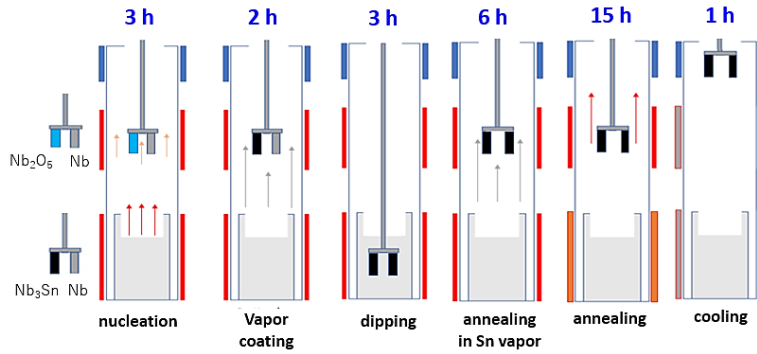
Fig. 2: On the left, the treated substrates and their changes in the various steps are shown. The picture shows the positioning of the samples in the process chamber during the various steps.
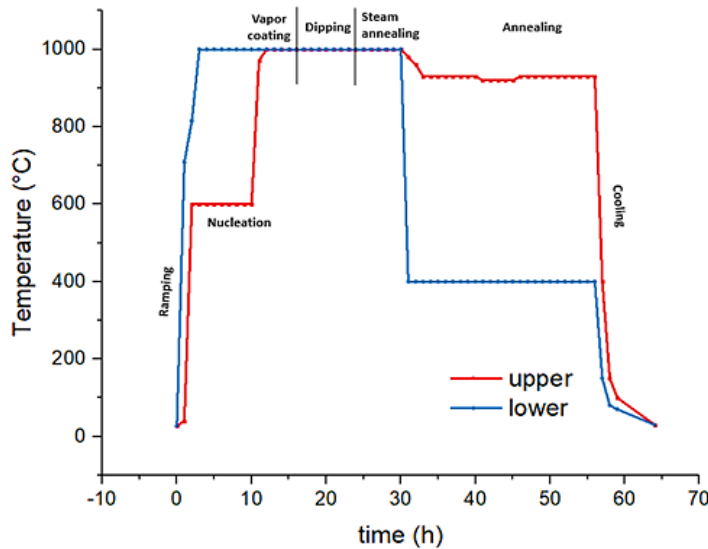
Fig. 3: Temperature profiles of furnaces in the complete process with nucleation step for targets synthesis.

Ramping: the lower furnace is switched on to obtain degassing of the crucible, an hour later the upper furnace is switched on.

Nucleation: the substrates are located at the centre of the chamber in the annealing zone and remain there for 3 to 9 h at 600∘C.

Coating: the upper furnace increases the temperature of the system to 1000∘C and remains at the same temperature from 2 to 9 h.

Dipping: The substrates are immersed in the molten tin at 1000∘C from 0.5 to 7 h by means of the feedthrough.

Steam annealing: the samples brought back to the centre of the chamber are heated from 7.5 to 77 h in the presence of the tin vapours of the crucible at 1000∘C.

Annealing: the lower furnace decreases in temperature to block the tin landing on the surface of the samples allowing annealing from 15 to 84 h at 1000°C.

Cooling: the samples are brought to the upper area of the water jacket to achieve thermal quenching of the material and avoid the formation of other unwanted phases.

2.1. DC Magnetron Sputtering System

The Direct Current Magnetron Sputtering (DCMS) system consists of an ultra-high vacuum pumping system, a 1-inch magnetron for housing the planar target obtained via LTD and a heatable sample holder. All the system is heated to 750°C and evacuated to a base pressure of 10^{-6} mbar. The second annealing after the sputtering process can be performed to increase A15 phase of the de-posited film.

3. Characterization

In this work, structural analyses are developed using diffraction in the goniometric mode. Morphological analyses were conducted with a scanning electron microscope with tungsten filament. Chemical analyses are carried out with the Energy Dispersive X-ray Spectrometry (EDS) instrumentation of LNL, while X-ray Photoelectron Spectroscopy (XPS) analyses were performed at the University of Padua. XPS measurements were carried out with a Perkin Elmer Φ 5600ci Multi Technique System. The spectra were collected with a standard Al Kα source and the peak positions were corrected for the charging effects by considering the C 1s peak at 285.0 eV and evaluating the BE differences.

4. Results and Discussion

The steps of the optimised LTD process were investigated and optimised. The following parameters were studied in the various experiments: the influence of the oxide layer (anodised Nb), the dipping time and the annealing time in the presence and absence of tin vapours.

The processes were first developed with BCP-treated Nb. Heat treatments in the presence and absence of steam allowed the evaluation of compositional changes on the surface and along the film. Since the aim is a thick film, the dipping time was increased to increase the thickness.

To improve the surface quality of the samples, it was decided to study the processes just described with the initial anodising treatment.

The morphological and structural characterization allows to understand the quality of the film obtained.

Process	Sample	Nucleation Step T(°C) t(h)	Coating Step T(°C) t(h)	Dipping T(°C) t(h)	Steam Annealing T(°C) t(h)	Annealing T(°C) t(h)
P1	C1-C2	600 2	1000 2	1000 3	1000 6	1000 15
P2	C3	/	/	1000 3	1000 21	/
P3	C4	/	/	1000 3	/	970 19
P4	C5	/	/	1000 3	1000 6	1000 15
P5	T1-T2	600 9	600 9	1000 5	1000 36	990 60

Fig. 4: Parameters used in Liquid Tin Diffusion process. C2 and T2 are anodized samples.

4.1. Sample Pre-treatment and Chemical Analysis

The formation of percolating pathways inside the material are the limit found in old processes without Nb anodization. This phenomenology leads to the consequent incorporation of tin on the surface and small sintering of the grains [3]. By evaluating the liquidus curve in the Nb_3Sn phase diagram under dipping conditions in Fig. 1 (Sn > 25% due to immersion in molten Sn and temperature > 930°C), it is observed that a fraction of niobium can be solubilized in the bath due to the simultaneous existence of the Nb_3Sn+liquid phase.
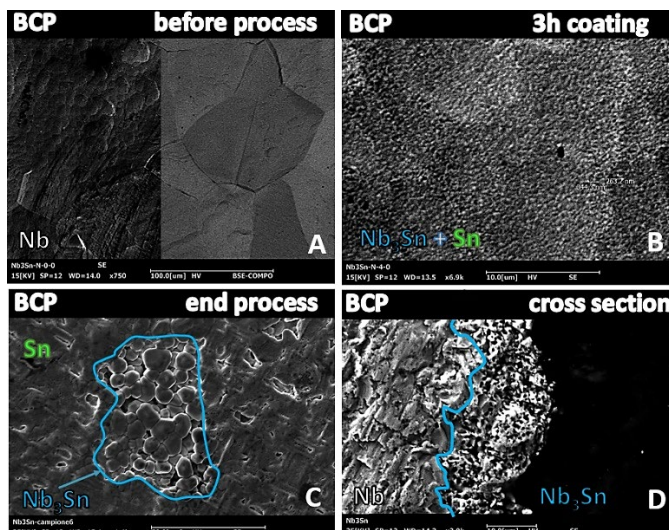
Fig. 5: SEM micrographs of the sample treated only with BCP before the process P1 (A), at the end of the coating phase (B) and complete process (C). Image (D) is the cross section of the sample in the section (C) cut at the end of the complete process.

The samples of process P1 described in Fig. 4 after BCP Fig. 5 (A) are subject to the immediate formation of approximately 6 nm of Nb_2O_5 when exposed to the atmosphere [9]. The niobium oxide layer is known to promote the formation of the desired A15 phase [4]. Half of the micrograph is obtained with the secondary electrons and the morphology of the Nb grains is visible, while the other half micrograph (right) is obtained with the backscattering electrons. From the micrographs in Fig 5 (B) it is possible to estimate a degree of coverage of 93 % with crystallites having an average size greater than 250 nm. The EDS analysis shows the presence of Sn from 17-30% in restrict areas indicating a sporadic uncontrolled nucleation.

In the micrograph Fig. 5 (C) the presence of unreacted Sn, which partially covers the surface is evident. In localized points, grains of Nb_3Sn (25-30% Sn) of about 10 microns are present, excess tin is often found in grain boundaries as shown in Fig. 6. The EDS depth elements profile is obtained evaluating the penetration length of the electron beam as a function of the material observed. Given the high temperature of the annealing step in the absence of steam, which continues for a long time, there is a degassing of the inconel chamber which promotes the formation of a layer rich in Cr. In this type of process, contamination is present between the grain boundaries of the different crystallites, while in the centre of the grain it is not detectable within the EDS limits. This contamination is not present in the surface areas covered by residual Sn.

From the SEM micrographs cross-section of the films without anodization, Fig. 5 (D) process P1, it is possible to observe the formation of percolation paths inside the film which determine a high porosity. For the realization of a target this would lead to a greater erosion of the film and inhomogeneity of the composition. The EDS profile of the cross section in Fig. 7 shows a non-monotonic variation of tin concentration within the film. This irregular pattern could be due to the trapping of tin, due to the formation of percolative paths.
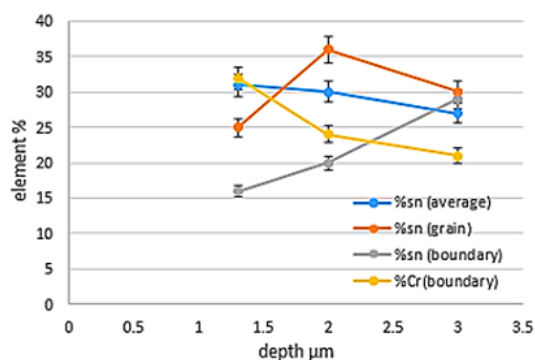
Fig. 6: EDS depth profile of Sn and Cr on the intra-grains (grain) and between inter-grains (boundary).
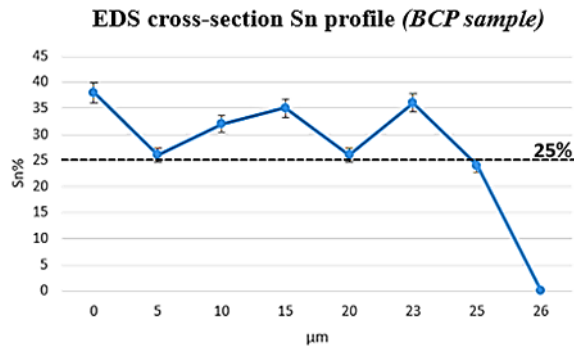
Fig. 7: EDS depth profile of Sn % on the cross section of BCP sample.

The samples subjected to the anodizing treatment , as in Fig. 8 (A) relative to P1 process described in Fig. 4, are treated to favour nucleation at 600°C. At the end of the coating step Nb_3Sn crystallites are growth before the dipping step as shown in Fig 8 (B). The growth allows a first coating of the sample surface similarly to VTD. From the analysis of the micrographs in Fig. 8 (B) it is possible to observe a coverage of 96 % with crystallites having an average size greater than 250 nm with good uniformity. The process is conducted without $SnCl_2$ nucleating agent, instead of what is usually done in the VTD. The EDS analysis provides Sn concentration of 24-25% in large areas indicating a controlled nucleation. The presence of A15 film before dip-ping renders the substrate insoluble, limiting the formation of percolation pathways.
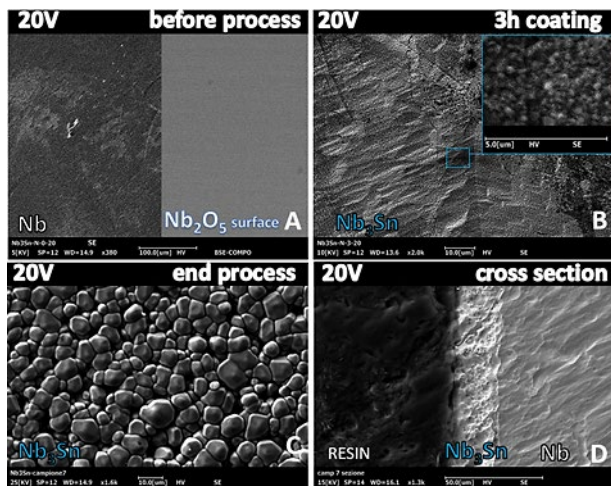

Fig. 8: SEM micrographs of the anodized sample before the process P1 (A), at the end of the coating phase (B), complete process (C). Image (D) is the cross section of the sample in the section (C) cut at the end of the complete process.

The Nb_2O_5 layer of the substrate has a beneficial effect on the whole process, in fact in Fig. 8 (C) Nb_3Sn grains are observed with correct stoichiometric composition and size larger than 8 microns. The Analysis of the elemental profile in Fig. 9 shows that the concentration of tin in the grain boundaries is slightly higher than the stoichiometric concentration. The diffusion occurs at the edge but there is no segregation of metallic Sn. The Sn concentration between the surface and the edges of the crystallite is comparable. The Cr contamination is still preferential along the grain boundaries and increases within the first micron in this area. The Niobium oxide may favour the migration of the Cr contaminant within the film.

The cross section of the film in Fig. 8 (D) shows a higher density when compared to the previous film (Fig. 5 D). The stoichiometry along the film decreases as the thickness increases Fig. 10; in the first few microns, a phase compatible with Nb_6Sn_5 is observed and then a concentration compatible with the A15 phase is obtained. The EDS analysis carried out on the section gives an average stoichiometry of the Nb-Sn system with a tin concentration of about 25%.

The diffractometric analysis confirms the A15 phase and agrees with the EDS results.

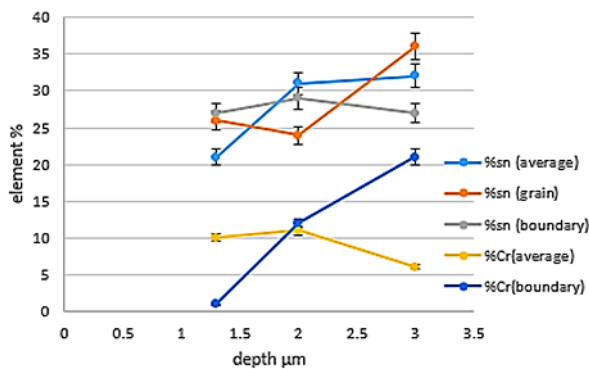**EDS depth element profile** *(Anodized sample)*

Fig. 9: EDS depth profile of Sn and Cr within the anodized sample.

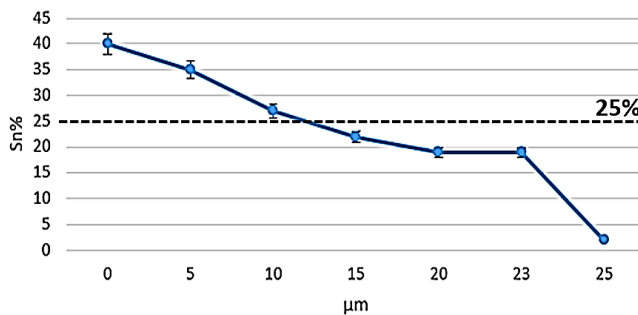**EDS cross-section Sn profile** *(Anodized sample)*

Fig. 10: EDS profile of Sn % on the cross section of anodized sample.

The XPS analysis in Fig. 11 investigates the chemical composition on the surface of the samples; they were sputtered through the ion gun for 1 minute and then the measurements were carried out. The BCP-treated sample shows less oxygen than the sample with the initial Nb_2O_5 layer (ΔO 3%) within the first 10 nm of the material, the investigation depth of these measurements by XPS. As already seen with the EDS analysis, the surface composition for the sample with BCP is Sn 28 % and the presence of Nb_3Sn is confirmed in addition to metallic Sn. The spectrum does not show Cr, the surface tin limits the diffusion of the contaminant.
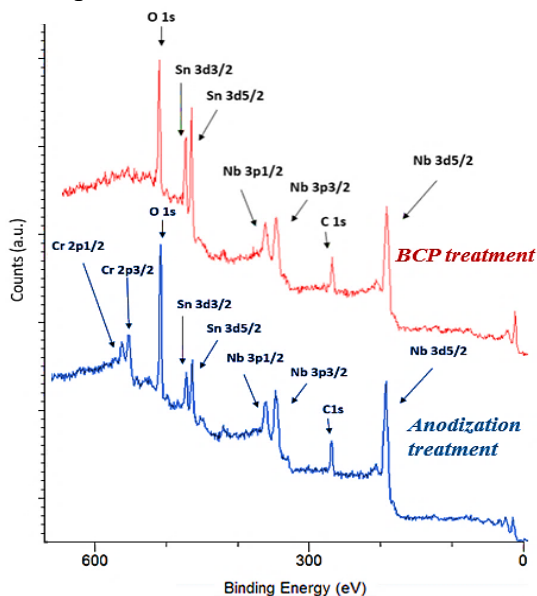

Fig. 11: XPS spectra after the same process for a BCP treated sample (red curve) and an anodized sample (blue curve).

The spectrum of the anodised sample shows Sn 19% stoichiometry of phase A15. The concentration is lower than that expected by EDS because a considerable amount of Cr 16% is detected by the peaks in 580 eV region. The niobium oxide as well as promoting the formation of the desired phase could allow an easier migration of the Cr within the film.

From the comparison of the samples subjected to the two initial superficial treatments (Only BCP and BCP plus anodization), it can be deduced that the formation of Nb$_3$Sn is promoted by the oxide layer. This can be estimated by the degree of surface coating and the stoichiometry of the material. A good coating before immersion allows the minimisation of unreacted tin on the surface and avoids the formation of microscopic paths. The absence of metallic tin and the presence of oxide also seem to increase the migration of the Cr contaminant along the grain boundary.

4.2. Dipping Time

The liquid diffusion processes are faster due to the higher diffusion coefficient and the establishment of new mechanisms at the grain boundaries as dissolution and eventual precipitation [3]. In the molten tin, the capillary pressure could greatly emphasise the transport of matter between the edges of the electronic compound. An increase in thickness is observed increasing the dipping time.

To maintain the stoichiometry along the film as the thickness increases, it is also necessary to increase the annealing time. In processes with global annealing times of less than 7 times the dipping time, a higher presence of Sn was found. The graph of the thickness obtainable as a function of immersion time is plotted in Fig. 12. Using the Fick's law, it is possible to obtain Eq. 1 for BCP samples and Eq. 2 for anodized samples with which it is possible to calculate the achievable thickness in a process.

$$x^2_{BCP}=156.7 \, t +129.5 \qquad \qquad \text{Eq. (1)}$$

$$x^2_{anodized}=159.6 \, t +0.9 \qquad \qquad \text{Eq. (2)}$$

Where x is the thickness expressed in μm and t the time expressed in hours.

The slopes are similar, indicating that the basic physical phenomenology is the same. As with VTD processes, the grain edge will drive the formation of the film. The molten material is likely to increase the mobility of chemical species in the system. The error in the plot is due to the variability of the thickness. In BCP samples there is a maximum deviation of 4 μm, while in anodized samples this decreases on average to 2 μm. The oxide seems to have a levelling effect during growth allowing an increase in thickness control.
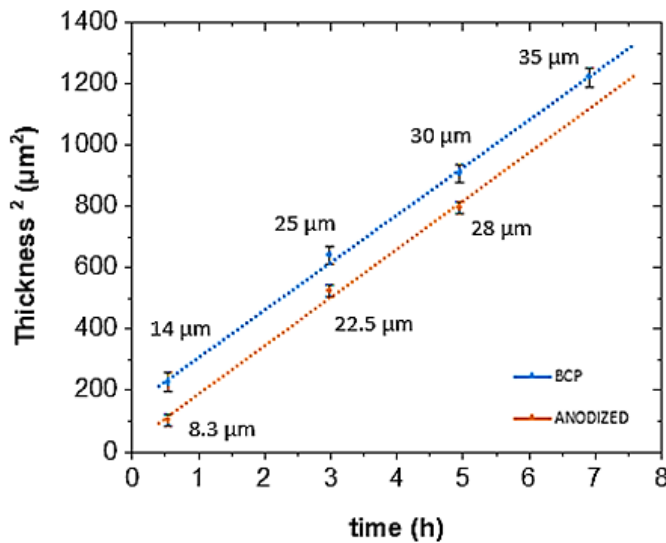
Fig. 12: Plot of the thickness as a function of the dipping time for the BCP non-anodized (blue) and anodized (orange) sample.

4.3. Annealing Time

The heat treatments with Sn steam vapour and without tin flux are essential to control the stoichiometry along the film. In process P2 Fig. 13 (A) metallic Sn remains on the surface due to the immersion step. The continuous steam vapour thermal treatments imply a difficulty in eliminating the macroscopic drops, but a stoichiometry of phase A15 of 24-25% is achieved. A non-uniform metallic tin layer is present on 52% of the surface.

The heat treatments without Sn steam lea d to minimizing the macroscopic drops. The sample relative to the process P3 is shown in Fig. 13 (B). This annealing without Sn steam provides a tin concentration lower than 23% in the A15 phase (from EDS and XRD analysis Fig. 14). A Sn layer with an average thickness of less than 500 nm is present on the surface. The high temperature of the annealing step determines an evaporation of Cr from walls of inconel chamber. A Cr layer of thickness below 500 nm and composition greater than 30% is present. The Cr contamination is present only where the Nb3Sn is exposed to surface and does not appear in areas covered by metallic Sn.

In the double annealing process P5 (Fig. 4) the annealing sequence, with Sn steam and after without, is used to first have a slow evaporation of the Sn while maintaining a correct stoichiometry, and consequently, to eliminate the residual tin and favour sintering. The macroscopic drops decreased, and the residual surface layer became the 94% of Nb_6Sn_5 phase coverage. The XRD and EDS characterizations relating to the sample shown in the micrograph in Fig. 13 (C), con-firm a concentration of 24-25%.

The formation of Nb_2O_5 layer with anodization treatment of the substrate plays a key role, in fact, in the same process, the double heat treatment involves the presence of only phase A15 at 24-25% as shown in Fig. 13 (D) coverage 96% (process P1 sample C2). The Cr contamination is higher (40%) than only BCP sample (30%). This phenomenology is due to the lower residual Sn.

From the diffractometric analysis in Fig. 14 it is evident how the heat treatments affect the phases obtained. With annealing in the continuous presence of steam, it is not possible to eliminate the residual Sn, which leads to $NbSn_2$. The prolonged annealing treatment leads the $NbSn_2$ phase to lose tin and become Nb_6Sn_5. The sequential heat treatment leads to the stoichiometric A15 phase minimising the others; moreover the anodization of the substrate reduces the spurious phases even near the surface.
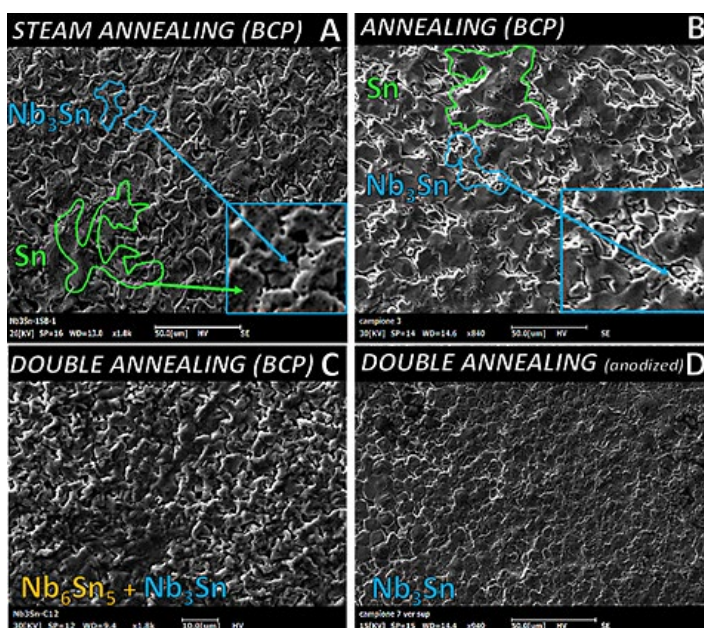
Fig. 13: SEM micrographs of samples treated only with BCP and subjected to heat treatments in the presence of steam (A), in the absence of steam (B), hybrid process (C) and influence of the hybrid process with substrate anodization.
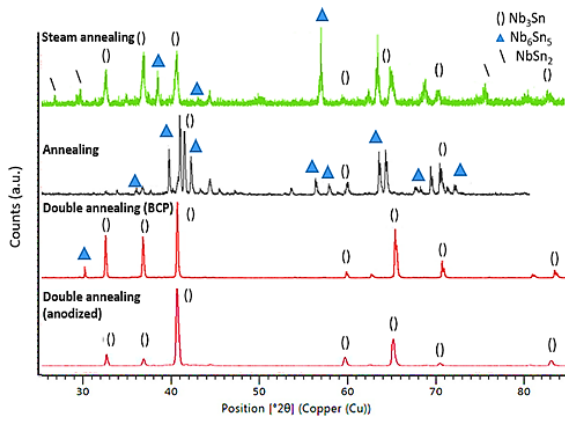
Fig. 14: XRD analysis of the samples treated with steam annealing (green), annealing without Sn vapour (black), double sequential annealing in sample without and with anodization (red).

4.4. Nb₃Sn Planar Target

Five 5 targets were synthesized, 4 were anodized (T2) and 1 were treated only with BCP (T1) with the process P5 (see Fig. 4).

In Fig. 15 relative to the anodized sample (T2), a surface contamination of Cr greater than 40% is observed. At the diffractometer, no Cr-containing phases are detected are present along the film. The average stoichiometry of the film is 26 % and the average thickness is 27 μm as expected.
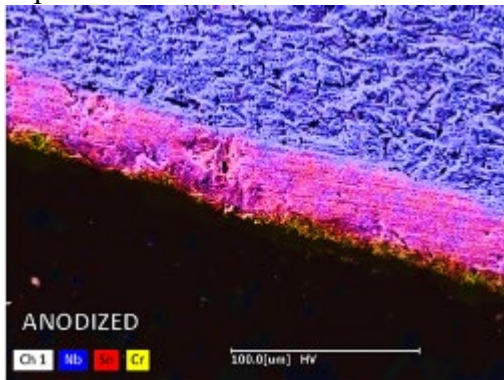
Fig. 15: SEM micrograph with EDS mapping of the target treated with BCP and subsequent anodization.

4.5. Nb₃Sn DC Magnetron Sputtering

The Fig. 16 resumes the sputtering process and the target used for Nb3Sn on quartz deposition. Only anodized targets have been used.

Working pressure (Ar)	Deposition time and current	Deposition temperature
Process		750°C plus 15 min after process
5*10-3 mbar	3min 0.1 A	

**Fig. 16**：Sputtering Parameters and Processes.

The objective is the deposition of 1 μm of Nb_3Sn on quartz with a Nb_3Sn thick film of 28 μm made via LTD.

The micrograph in Fig. 17 A shows the surface of the target before DCMS. In Fig. 17 (B) it is possible to observe the rail track after the sputtering process. From the compositional analysis, only the presence of Nb is observed along the trace. This means that more of the available Nb_3Sn film has been sputtered out. The process was stopped when a change in voltage was observed, indicating a change in the sputtered material. The XRD pattern show a stoichiometry of 24.5-25% for A15 phase and a small presence of Nb_6Sn_5 spurious phase Fig. 18 (red). The EDS shows a global average of Sn 28%. The coating is visible in Fig. 17 (C). The

film is 1.2 μm thick (measured by profilometer, deposition rate 40 nm/min) with a Sn concentration on the grains of 25-26% with a grains average size of 250 nm; there are clusters of Nb with a size greater than 400 nm in localized areas. The EDS map of the deposited film is presented in the micrograph (D). The EDS characterization provides a global stoichiometry with Sn 20% confirming the presence of localized Nb. The XRD comparison of the sputtered film in Fig. 18 (black) shows the same phase as the initial target film (red), no Cr species are detected.
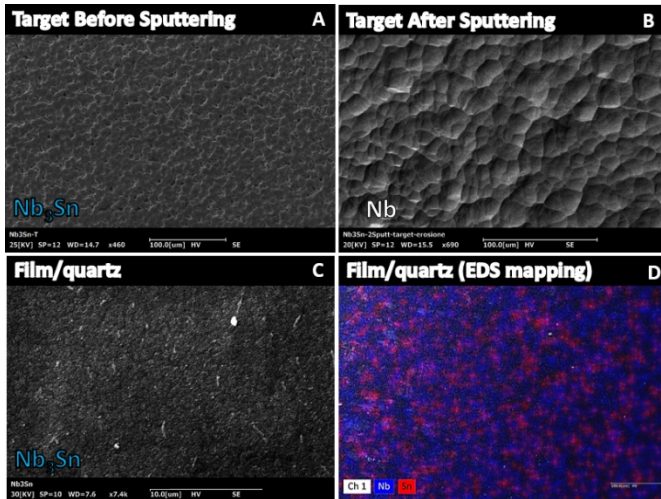
Fig. 17: SEM micrographs of the targets before sputtering process (A) and rail track after the process (B). Nb$_3$Sn deposition on quartz (C) and EDS mapping (D).
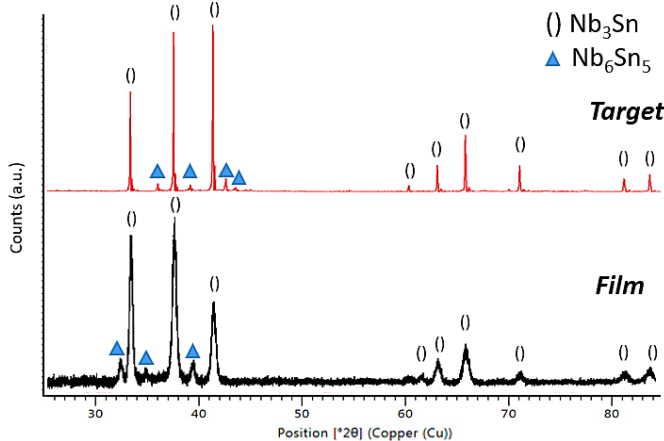
Fig. 18: XRD of the target before DCMS (red) and XRD of the deposit film (black).

5. Conclusions

The controlled nucleation obtained by substrate anodization is fundamental to improve the film quality. This process reduces macroscopic tin droplets and spurious phases allowing a better maintenance of the ideal stoichiometry of 25% of Sn in the A15 structure.

The dipping time is the main factor that affects the film thickness. The relationships found with Fick's law allow to estimate the thickness. The 5 hours processes allow to obtain 28 μm Nb$_3$Sn film in the target sufficient for the deposition of 1 μm of Nb$_3$Sn via DCMS sputtering.

The sequential double annealing heat treatment is essential to obtain a correct stoichiometry and has been used as a standard for the manufacture of single-use Nb$_3$Sn planar targets.

The single-use Nb$_3$Sn planar targets were successfully tested growing 1 μm of film via DCMS sputtering on quartz substrates.

The characterization of the sputtered film on quartz confirms the A15 phase in the coating.

In the future a niobium screen will be introduced inside the chamber to eliminate/reduce chromium contamination in the LTD process. The LTD optimized process will be tested on cylindrical cathodes and systematic study on sputtering deposition parameters will be performed.

Acknowledgements

References

[1] E. A. Ilyina et al., "Development of sputtered Nb_3Sn films on copper substrates for superconducting radiofrequency applications", Supercond. Sci. Technol., vol. 32, no. 3, p. 035002, 2019. https://doi.org/10.1088/13616668/aaf61f

[2] S. M Deambrosis et al., "A15 superconductors: An alternative to niobium for RF cavities", Physica C, vol. 441, iss. 1-2, pp. 108-113, 2006. https://doi.org/10.1016/j.physc.2006.03.047

[3] M. Zanierato, "Studio e sviluppo delle tecniche di deposizione di film sottili di Nb_3Sn per applicazioni in cavità risonanti", Master's Degree Thesis, Department of Chemical Science, University of Padua, Italy, 2020.

[4] S. Posen et al., «Advances in Nb_3Sn superconducting radiofrequency cavities towards first practical accelerator applications», Supercond. Sci. Technol., vol. 34, n. 2, pag. 025007, feb. 2021, doi: 10.1088/1361-6668/abc7f7.

[5] Sayeed, Md Nizam, et al. "Structural and superconducting properties of Nb_3Sn films grown by multilayer sequential magnetron sputtering." Journal of Alloys and Compounds 800 (2019): 272-278.

[6] Wu, C. T., R. T. Kampwirth, and J. W. Hafstrom. "High-rate magnetron sputtering of high Tc Nb_3Sn films." Journal of Vacuum Science and Technology 14.1 (1977): 134-137.

[7] A. Godeke, "A review of the properties of Nb3Sn and their variation with A15 composition, morphology and strain state", Supercond. Sci. Technol., vol. 19, no. 8, p. R68, 2006. https://doi.org/10.1088/0953-2048/19/8/R02

[8] Boffo, Cristian, et al. Optimization of the BCP processing of elliptical Nb SRF cavities. No. FERMILAB-CONF-06-181-TD. Fermi National Accelerator Lab.(FNAL), Batavia, IL (United States), 2006.

[9] Bach, David. "EELS investigations of stoichiometric niobium oxides and niobium-based capacitors." (2009).